Functional Dependence of Cancellous Bone Shear Properties on Trabecular Microstructure Evaluated Using Time-Lapsed Micro-Computed Tomographic Imaging and Torsion Testing

Ara Nazarian,[1,2] Diego Meier,[1,2] Ralph Müller,[1,2,3] Brian D. Snyder[1,4]

[1]Orthopedic Biomechanics Laboratory (OBL), Beth Israel Deaconess Medical Center and Harvard Medical School, Boston, Massachusetts, [2]Institute for Biomedical Engineering, University and ETH Zürich, Zürich, Switzerland, [3]Institute for Biomechanics, Swiss Federal Institute of Technology, Zürich, Switzerland, [4]Department of Orthopaedic Surgery, Children's Hospital, Harvard Medical School, Boston, Massachusetts

Received 26 October 2007; accepted 4 May 2009
Published online in Wiley InterScience (www.interscience.wiley.com). DOI 10.1002/jor.20931

ABSTRACT: When compressed axially, cancellous bone often fails at an oblique angle along well-defined bands, highlighting the importance of cancellous bone shear properties. Torsion testing to determine shear properties of cancellous bone has often been conducted under conditions appropriate only for axisymmetric specimens comprised of homogeneous and isotropic materials. However, most cancellous bone specimens do not meet these stringent test conditions. Therefore, we studied the application of the stepwise torsion testing system in biologic specimens with viscoelastic behavior. We explore the functional dependence of cancellous bone shear properties on trabecular microstructure and its spatial distribution, specifically the contribution of the subregion with the minimum polar moment of inertia to the overall failure properties. Torsional properties of whale trabecular specimens obtained by the incremental application of stepwise torque were not different from those obtained via continuous testing. Average polar moment of inertia accounted for 82 and 67% of the variation in shear modulus and shear stress, respectively. However, torsional properties were better predicted by the subregion with minimum polar moment of inertia, describing 87 and 74% of the variation in shear modulus and shear stress. The use of a novel torsion testing system for nonhomogeneous, orthotropic cancellous bone using stepwise application of torsion and simultaneous micro-computed tomographic imaging was further studied. Most importantly, a heterogeneous cancellous bone microstructural environment, the subregion with the minimum polar moment of inertia, hence the weakest spatial distribution of bone, predicted the shear properties for the entire bone volume. © 2009 Orthopaedic Research Society. Published by Wiley Periodicals, Inc. J Orthop Res

Keywords: cancellous bone; torsion testing; shear properties; micro-computed tomography

An understanding of the relationship between cancellous bone microstructure and its function is essential for determining nontraumatic fracture risk associated with metabolic bone diseases. In turn, understanding of fracture risks will result in optimizing pharmacological interventions to enhance bone remodeling by blocking resorption and/or promoting formation. Relationships between material properties (strength and stiffness) and trabecular microstructure have been established for normal and pathologic human and animal bone specimens loaded in tension or compression.[1–13] Also, we introduced time-lapsed micro-computed tomographic (μCT) imaging and compression of cancellous bone to evaluate failure modes for whale (mostly platelike trabeculae) and human bones (mostly rodlike trabeculae).[14,15] When compressed axially, cancellous bone specimens often fail along well-defined bands at an oblique angle to the longitudinal axis, implying a contribution of shear to the failure mechanism.[16,17]

Previous researchers measured shear properties of cancellous bone,[18–22] but many of the tests were conducted under conditions appropriate only for axisymmetric specimens comprised of homogeneous and isotropic materials.[23,24] If a nonaxisymmetric, orthotropic specimen is subjected to torsion, it will warp and bend out of plane due to coupling between the mutually orthogonal normal and shear strains induced by the applied torque[25] (Fig. 1). If both ends of a nonaxisymmetric specimen are coaxially fixed to the load frame during testing,[21,24,26,27] the free movement of the specimen's neutral axis is restricted. When torque is applied along the centroidal axis, the loading profile is contaminated by additional (and unaccounted) bending moments that restrict out-of-plane deformation. To address this problem, we designed and validated a uniaxial torsional testing system for nonhomogeneous orthotropic or nonaxisymmetric specimens that accommodates out-of-plane warping and bending.[28] The system includes time-lapsed μCT imaging of the trabecular microstructure to visualize progressive deformation. We hypothesized that the system provides comparable torsional properties to those obtained from conventional testing and that the segment with the minimum trabecular spatial distribution best describes cancellous bone torsional properties.

METHODS

Specimen Preparation

The system has been described elsewhere.[28] Thirty cylindrical cancellous bone specimens (Ø: 7.82 ± 0.08 mm; H: 20.57 ± 0.14 mm) of similar mass and bone volume fraction were cored from the vertebral body of a Bowhead whale (*Balaena mysticetus*) along the cephalo-caudal axis using a diamond-tipped coring tool (Starlite Industries, Rosemont, PA). Measures were taken to minimize disruption of the trabecular network and to keep the specimen fully hydrated during coring by keeping the vertebra submerged in a 0.9% saline bath. Both ends of the cored specimens were cut perpendicular to the predominant direction of trabecular orientation using a low-speed saw (Isomet; Buehler Corp., Lake Bluff, IL) with two parallel diamond-tipped wafering

Correspondence to: Brian D. Snyder (Telephone: 617-667-2940; Fax: 617-667-7175; E-mail: bsnyder@bidmc.harvard.edu)

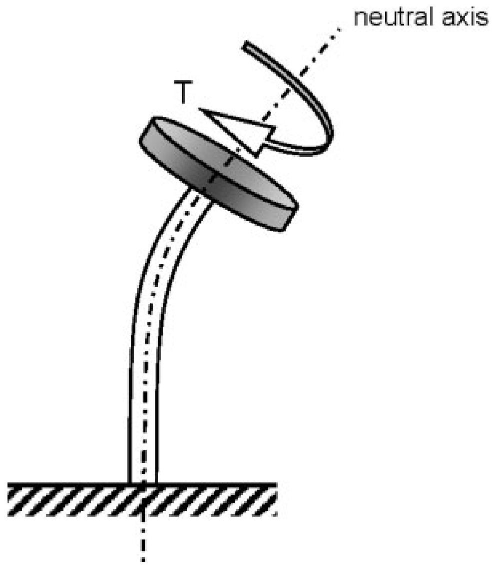

Figure 1. A schematic view of out-of-plane warping and bending due to torsion.

blades under copious irrigation. The specimens were placed in a water-filled vial inside a sonic agitator (Solid State/Ultrasonic FS-14; Fisher Scientific, Pittsburgh, PA) for 30 min and centrifuged at $8 \times g$ for 15 min to remove bone marrow and debris. The wet mass along with height and diameter were recorded. Eight pairs of specimens matched by mass (2.15 ± 0.16 g and 2.19 ± 0.16 g) and bone volume fraction (0.40 ± 0.06 and 0.40 ± 0.03) were randomly assigned to undergo torsional testing at a continuous ramp (CONT) or incremental stepwise function (SW) to an angular displacement of 25°.

μCT Imaging and Analysis

Sequential, cross-sectional images of the specimens were acquired using a μCT 40 (Scanco Medical AG, Brüttisellen, Switzerland) at 70 kVp tube voltage, 114 μA tube current, 250 ms integration time, and 30 μm isotropic voxel size. A 3D Gaussian filter ($\sigma = 0.8$) with limited finite filter support (support = 1) was used to suppress noise. Images were thresholded to separate bone from background using an adaptive algorithm.

Each image was divided into 10 axial subregions of equal height to evaluate the relative heterogeneity of the bone volume fraction and microstructure (Fig. 2). Three dimensional

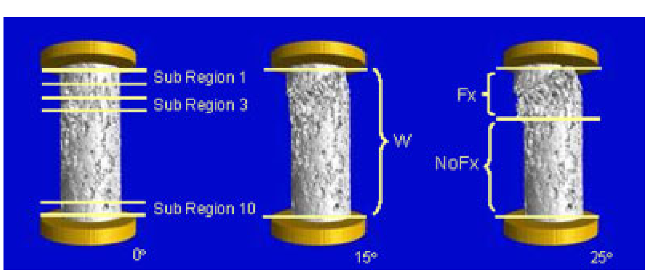

Figure 2. Torsion steps of 0°, 15°, and 25° angular displacements (left to right) from a representative specimen. The failure region (FX), the nonfailure region (NF), and the whole specimen (W) are identified on the 25° and 15° images; the equal subregions (SR1–10) are highlighted on the intact whole specimen.

structural indices were computed for the specimen and for each subregion: bone volume fraction (BV/TV, mm^3/mm^3), bone surface density (BS/TV, mm^2/mm^3), specific bone surface (BS/BV, mm^2/mm^3), trabecular number ($Tb \cdot N$, mm^{-1}), trabecular thickness ($Tb \cdot Th$, mm), trabecular spacing ($Tb \cdot Sp$, mm), connectivity density ($Conn \cdot D$, mm^{-3}), degree of anisotropy (DA), and structure model index (SMI). Bone mineral density (ρ) of the specimen was also calculated using hydroxyapatite (HA) phantoms of 100, 200, 400, and 800 mg $HA \cdot cm^{-3}$ density. Average (J) and minimum (J_{MIN}) polar moments of inertia were calculated. ρ and J products ($J.\rho$ and $J_{MIN}.\rho$) were calculated as surrogates of bone density and its distribution along the longitudinal axis.

Three dimensional incremental images of each test were compiled into an animation. Images were aligned initially with respect to the bottom end plate, which was fixed during the experiment. Each aligned dataset was visualized under the same orientation and light setting conditions using an extended Marching Cubes algorithm.[29] Failure (Fx) and nonfailure (NoFx) regions were established from the front, back, left, and right viewing angles by two independent observers who viewed the animations through a subregion delineation mask. The subregion where the trabecular network had undergone damage was assigned as Fx and the remainder as NoFx.

Mechanical Testing

Specimen ends were embedded in polymethylmethacrylate (PMMA) end-caps to facilitate gripping and minimize crushing that might damage the specimen during testing. Specimens were mounted in the test system, and incremental stepwise or continuous angular displacement to failure was applied under displacement control.

Stepwise incremental (SW) testing consisted of μCT imaging at zero angular displacement, followed by application of displacements of 0.13 (7.5°), 0.26 (15°), 0.35 (20°), and 0.44 radians (25°) with μCT imaging at the conclusion of each step. Following each step, the specimen was allowed to relax for 20 min prior to transfer to the μCT (imaging duration ~60 min). The 20 min window was based on experiments performed to establish an appropriate time interval for stress relaxation. Stepwise angular displacement–torque diagrams consisted of three discrete sections between the four angular displacement steps. To obtain a continuous diagram, the end point of each section was connected to the beginning point of the next section via a straight line (dashed lines in Fig. 3a), assuming that results obtained from the reconstructed stepwise tests would be compatible with those obtained from continuous tests. This arbitrary method was used successfully in stepwise compression.[14,15]

Continuous testing consisted of applying angular displacement of 0.44 radians (25°). Both CONT and SW tests were performed at an angular displacement rate of 0.083 $rad \cdot s^{-1}$. Torque (T_{ULT}, $N \cdot m$) and angular displacement were measured and shear strength (σ_{ULT}, MPa) and strain (γ_{ULT}) were calculated using previously established methods[30]; torsional stiffness (K_{TOR}, $N \cdot m \cdot rad^{-1}$) and shear elastic modulus (G, MPa) were assessed from the linear portions of the angular displacement versus torsion and shear strain versus stress curves, respectively. Specimens remained hydrated during testing, verified at the end of each test.

Statistical Analysis

The observers' independent assessments of failure regions were compared to established failure regions. Intraclass

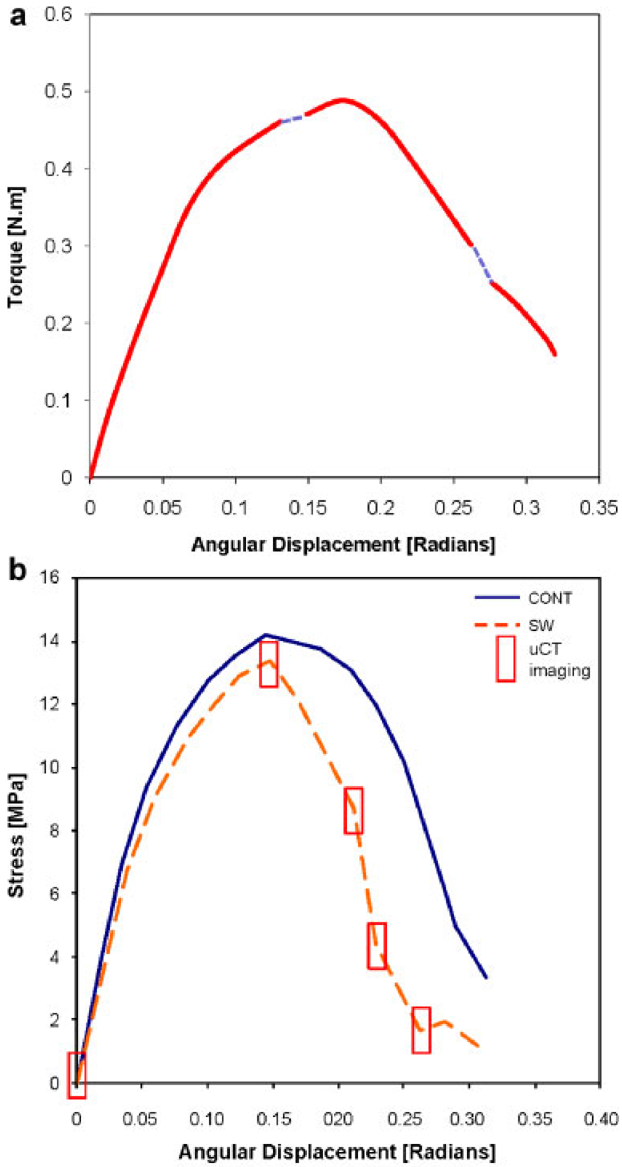

Figure 3. Reconstruction of a stepwise test figure for further analysis (a), and representative curves from stepwise and continuous application of angular displacement (b).

correlation was used to evaluate agreement between observers employing a one-way random model.

A two-tailed homoscedastic Student's t-test was performed to compare microstructural indices and torsional properties measured through CONT and SW testing. Correlations between SW and CONT torsional properties were assessed using linear regression analysis. Furthermore, ANOVA with Bonferroni posthoc test was performed to assess differences in trabecular indices (dependent variables) obtained from the whole specimen (W), Fx, and NoFx. Linear regression analysis was used to establish relations between torsional properties and microstructural indices.

The coefficient of determination (R^2) was used to compare different regression models obtained using average and minimum BV/TV and J. Our strategy was based on the Fisher r-to-z transformation with a back-transformation of the bounds to produce a 95% confidence interval (CI) for the difference between the correlations being compared. This strategy includes the 95% CI and Z test with a two-sided p value to test for differences between the correlations.[31,32]

The SPSS statistical package (version 15.0; Chicago, IL) was used for data analysis. All reported p values are two-tailed with $p < 0.05$ considered significant.

RESULTS

The SW torsional properties were not significantly different from the CONT properties (Table 1, Fig. 3b). Linear regression analysis revealed 79, 82, 92, 94, and 95% correlation between angular displacement, torque, ultimate strength (Fig. 4a), torsional stiffness and shear modulus of elasticity (Fig. 4b), respectively. No differences were observed in standard 3D microstructural indices between W, Fx, and NoFx ($p > 0.05$ for all cases, Table 2).

The BV/TV values averaged over the entire specimen accounted for 33 and 43% of the variation in G and T_{ULT}. However, G and T_{ULT} were better predicted by the subregion with the minimum BV/TV (BV/TV$_{MIN}$), accounting for 42 and 51% of the variations ($p < 0.05$).

$J.\rho$ accounted for 82 and 67% of the variation in G and T_{ULT} (Fig. 5a,b). But, G and T_{ULT} were better predicted by $J_{MIN}.\rho$, accounting for 87 and 74% of the variations (Fig. 5c,d; $p < 0.05$).

SMI, Tb · Th, and Conn · D described 40 (inverse), 42, and 51% of the variation in G. Other microstructural parameters did not provide a meaningful description of torsional behavior.

Intraclass correlation analysis of the failure regions suggested no observer effect (correlation 0.91). Visual observation of the animations generated from incremental μCT images revealed an initial pattern of trabecular bending, also reported by Fenech et al.,[33] at distinct shear failure lines followed by disconnection of

Table 1. Average Specimen and Mechanical Properties for Whale Cancellous Bone Specimens Undergoing Wither Conventional Continuous or Stepwise Torsion Testing

	Mass (g)	BV/TV (mm^3/mm^3)	Max Torque (N · m)	Ultimate Shear Strength (MPa)	Shear Modulus (MPa)
Average continuous SD	2.17 (0.18)	0.40 (0.06)	4.68 E-4 (0.4 E-4)	18.05 (2.88)	398.57 (49.64)
Average stepwise test SD	2.19 (0.15)	0.40 (0.03)	4.58 E-4 (0.4 E-4)	17.13 (2.)	374.02 (45.89)
Percent diff. (%)	1.9	0.8	2.1	5.1	6.2
p value	0.62	0.85	0.66	0.51	0.36

Mean and standard deviation (SD) in parentheses.

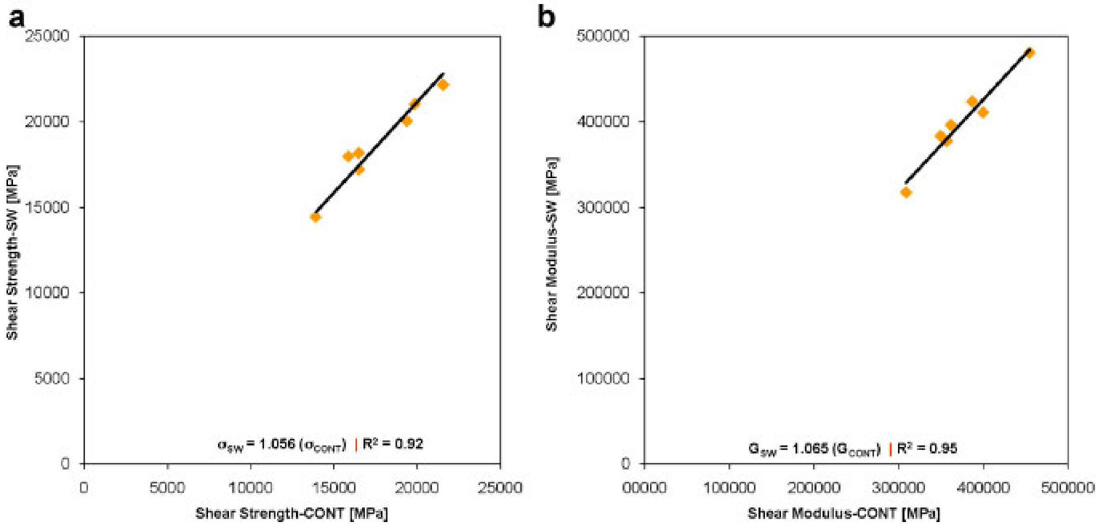

Figure 4. Correlation of stepwise and continuous shear strength (a) and modulus (b) values.

trabecular elements from the specimen under increasing angular displacement, resulting in a catastrophic burst failure and separation of a portion of the cancellous bone in the failure region. In a representative specimen (Fig. 6), bending of the individual trabecula (triangle marker) can be observed, followed by shear-induced disconnection of trabecular elements from their bases (square and circle markers).

DISCUSSION

Our first aim was to study the application of the stepwise torsion testing system in biologic specimens with viscoelastic behavior. Stepwise application of angular displacement yielded similar torsional properties as continuous torque application in a conventional torsion study ($p > 0.36$ for all cases). The shapes of the torque-displacement curves were not different from one another up to yield (Fig. 3b). This technique was employed previously to generate stepwise load displacement curves in uniaxial compression[15,34] of cancellous bone specimens from the same whale. Current findings indicate that torsional ultimate strength was 87.5% of the compressive ultimate strength, and average shear modulus of elasticity was 54% of the previously reported elastic modulus. Moreover, linear regression analysis between mechanical properties obtained from stepwise and continuous testing methods had correlations from 79 to 95%. The stepwise testing method, therefore, provided comparable torsional properties to those obtained through conventional continuous testing in orthotropic, nonaxisymmetric, and inhomogeneous cancellous bone specimens.

We performed displacement control twisting and pure torsion tests on three pairs of similar specimens and found an underestimation of 19 and 12%, respectively, for shear modulus and ultimate shear strength in the twisting cases. This finding further emphasizes the need for a more accurate bone torsion testing methodology.

Our second aim was to explore the functional dependence of shear properties on trabecular microstructure and its spatial distribution, namely the contribution of the subregion with the minimum polar moment of inertia to the overall failure properties. Treating the specimen as a series of stacked subregions along the length provided an opportunity to use a key aspect of torsion testing, where angular displacement is applied uniformly across the specimen length.

Given the narrow bone volume fraction range associated with these specimens, BV/TV described 32 and 43% of the shear modulus and ultimate strength, respectively. This prediction was improved when the region with the lowest bone volume fraction was used to describe 42 and 50%, respectively, of the variation in modulus and strength of the entire specimen. Therefore, the scalar parameter of amount of bone present, whether averaged over the entire specimen or at the least dense segment, at best provided a moderate description of the torsional properties of these specimens. However, the product of bone mineral density and polar moment of inertia, used as a surrogate of bone density and its spatial distribution along the longitudinal axis, strongly described the torsional properties, demonstrating the importance of the weakest region (material distribution to best resist the applied displacement/force) with respect to a specific loading mode.

Overall, the spatial distribution of bone around the torsion axis, and not the scalar amount of bone present described the torsional behavior of the whale cancellous bone. However, other microstructural parameters provide further insight into the failure modes. Trabecular thickness described about 40% of the shear modulus (i.e., increased thickness led to increased strength), yet trabecular number was not a significant descriptor of mechanical behavior (<15%). So, the amount of bone in the weakest subregion serves the strength in the form of increased trabecular thickness, not trabecular number. This is further verified by the inverse relationship

Table 2. Standard 3D Morphometric Indices of Whale Cancellous Bone Specimens Averaged Over the Entire Specimen (W), the Fracture Region (Fx), and the Nonfracture Region (NoFx)

	BV/TV (mm^3/mm^3)	BS/TV (mm^2/mm^3)	BS/BV (mm^2/mm^3)	Tb · N (1/mm)	Tb · Th (mm)	Tb · Sp (mm)	Conn-D. ($1/mm^3$)	DA	SMI
Whole specimen (W)	0.566 (0.107)	3.121 (0.227)	5.734 (1.327)	1.56 (0.114)	0.362 (0.067)	0.281 (0.087)	3.479 (0.878)	2.128 (0.116)	−2.097 (1.189)
Fracture region (Fx)	0.527 (0.146)	3.028 (0.193)	6.265 (2.159)	1.514 (0.096)	0.35 (0.105)	0.312 (0.095)	3.089 (0.892)	2.152 (0.168)	−1.855 (1.99)
Nonfracture region (NoFx)	0.502 (0.129)	3.167 (0.264)	6.723 (1.883)	1.584 (0.132)	0.318 (0.087)	0.317 (0.091)	3.901 (1.295)	2.211 (0.131)	−1.294 (1.467)
p value*	0.61	0.48	0.56	0.48	0.59	0.71	0.32	0.49	0.59

*p values for Bonferroni posthoc testing were in the range of $0.20 < p < 0.99$ for all cases. Mean and standard deviation (SD) in parentheses.

between structural model index and torsional properties, where a thicker, more platelike structure (lower SMI) provided a better prediction. Also, connectivity density, for which a higher number is associated with a more rodlike structure, described 51% of the variation in shear modulus. Structurally, a thicker, more platelike structure in the weakest subregion indicates a stronger specimen, consistent with the visual observations of the μCT-generated animations, where trabeculae disconnected (sheared) at the base under increasing angular displacement.

The subregion with the lowest bone volume fraction provided the smallest cross-sectional area and hence the weakest structural link in compression and tension. In torsion, this subregion has thinner trabecular elements and hence is a weaker segment. In bones undergoing metabolic changes, decreases in trabecular thickness could result in increased shear failure, because shear properties of cancellous bone are on average lower than compressive properties. In both compression and torsion, local failure bands are observed, where shear propagation is important in the overall failure of the specimen. In compression, this is mostly manifested as buckling of the elements, whereas in torsion, it is manifested as bending and shear failure of the elements at their base. However, the spatial distribution of material along the torsion axis is by far the most important factor in resisting torsional deformation.

Other researchers studied the torsional behavior of cancellous bone in bovine,[35–37] ovine,[27] canine,[38] ewe,[39] and human[19,23,40] with shear strength in the range of 3.1–7.7 MPa and shear modulus in the range of 263–366 MPa. Stone et al.[37] reported ultimate strength of 6.60 MPa for bovine proximal humeral cancellous bone. Ashman et al.,[35] using ultrasound techniques, presented shear modulus values of 333 and 311 MPa for bovine proximal and distal femoral cancellous bones. Ford[36] reported ultimate strength and shear modulus of 6.35 MPa and 349 MPa, respectively, for bovine proximal tibial cancellous bone. Kasra and Grynpas[27] performed torsion testing on ovine vertebral cancellous bones, reporting shear strength in the range of 4.8–7.7 MPa and shear modulus in the range of 263 to 366 MPa. In a computational study, Eswaran et al.[38] reported tissue-normalized strength of 3.1 MPa for canine vertebral cancellous bone. Mitton et al.[39] performed torsion testing on ewe vertebral cancellous bone, reporting shear strength of 5.3 MPa and 7.5 MPa for torsion testing at room temperature and at 37°C, respectively. Halawa et al.[19] reported human cancellous bone shear strength in the range of 4 to 5 MPA, and Bruyère Garnier et al.[23] reported ultimate stress and shear modulus of 6.1 MPa and 289 MPa, respectively, for human femoral cancellous bone specimens. Finally, Saha et al.[40] reported ultimate strength of 4.64 MPa and 3.65 MPa for embalmed human proximal and distal femoral cancellous bone. Our shear moduli for continuous and stepwise tests (374 and 389 MPa) are slightly higher than observed by other researchers, partially due to errors associated with the

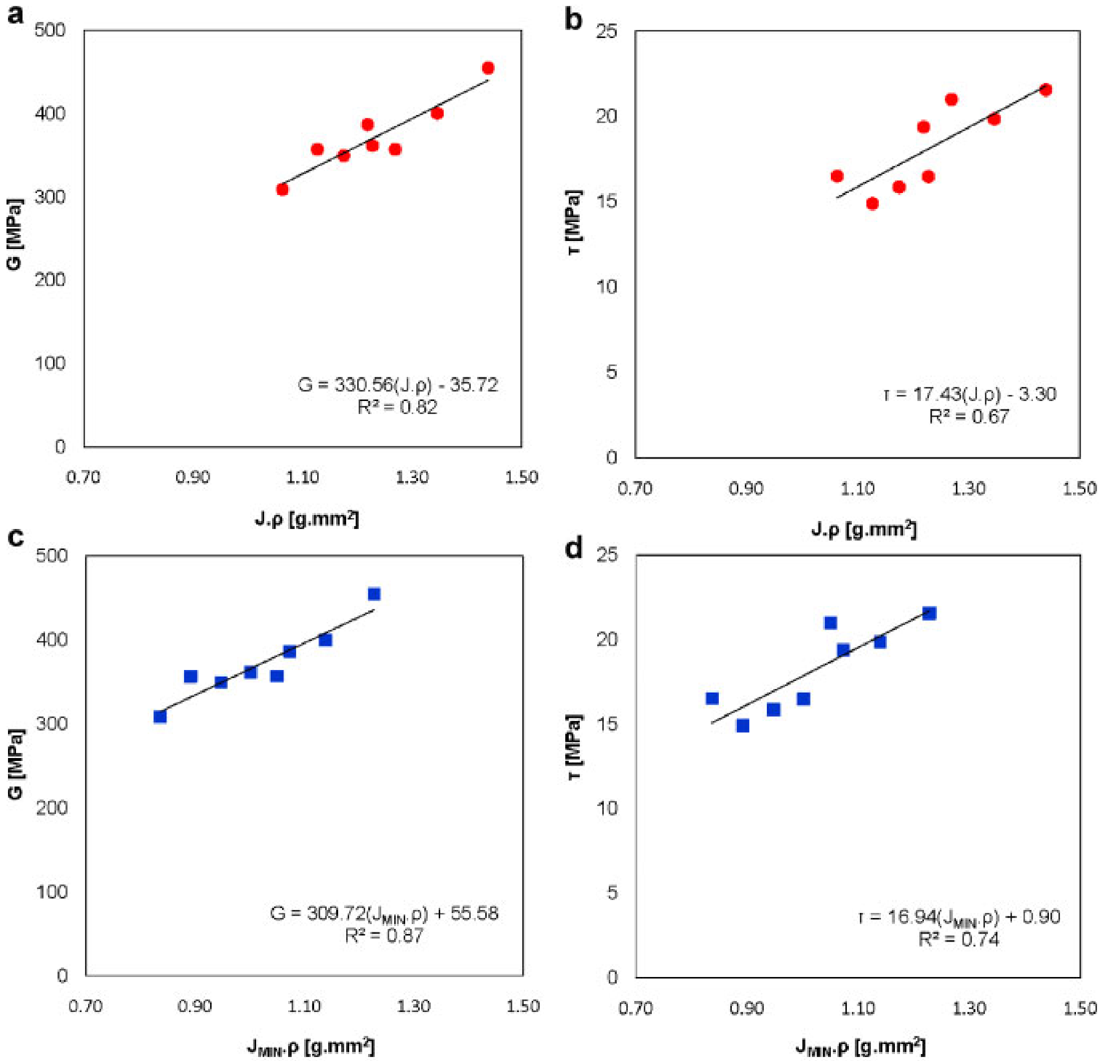

Figure 5. Shear modulus, shear strength, and torsional rigidity explained by the product of bone mineral density and polar moment of inertia averaged over the entire specimen (a,b) and the subregion with the minimum polar moment of inertia (c,d).

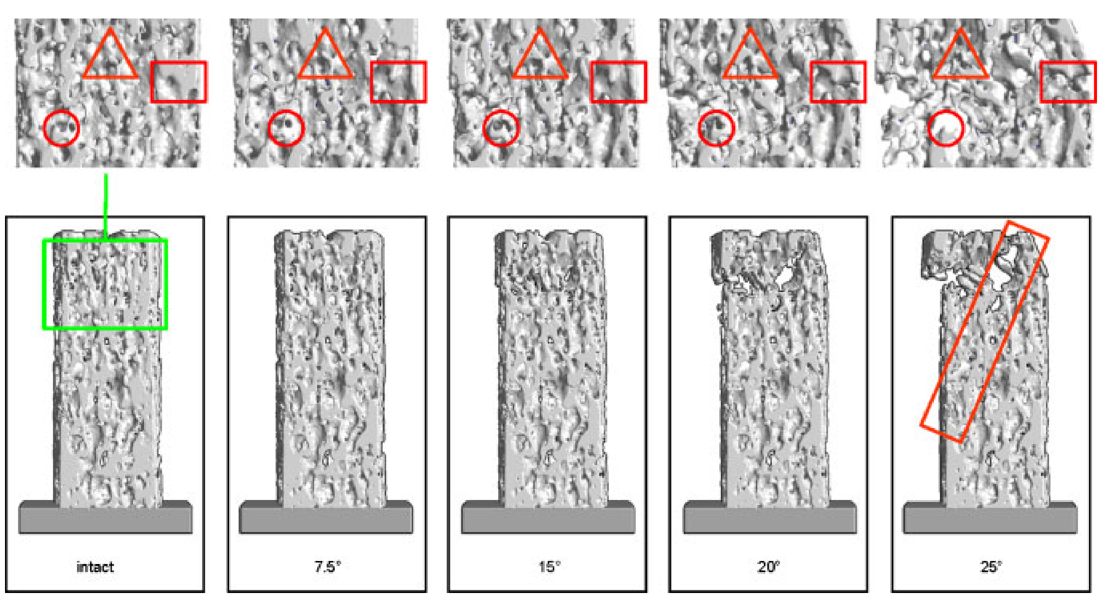

Figure 6. Torsion steps of 0° (intact), 7.5°, 15°, 20°, and 25° angular displacement on a representative specimen on a coronal view to see failure patterns. The red box super-imposed on the 25° image highlights the shear failure plane observed in the specimen. Detailed views of the upper portion of the specimen highlight failure patterns of the individual trabeculae.

twisting testing performed by other researchers and partially due to the higher bone volume fraction of whale cancellous bone. Our ultimate shear strengths (18.72 and 17.65 MPa) are about twice as large as those observed by others. Again, this discrepancy can be partly explained by the errors associated with the twisting testing and partially by the analysis method to assess ultimate strength. In our study, the largest strength values from each test were used as the ultimate strength, resulting in higher values than those using other methods.

The μCT-based animations revealed strong influence of bending and shear at the trabecular level followed by formation of shear failure lines at the specimen level. The eventual failure of the trabecular microstructure resulted in catastrophic fracture of the specimen under increasing angular displacement. The postyield behavior of the trabecular elements is important, because these elements maintain union under significant local axial displacement in compression or angular displacement in torsion. The ability to maintain union postyield is a critical ability of cancellous bone in responding to global and local displacement while maintaining connectivity within the tissue. The deformation/failure process was observed in an in vitro specimen; the behavior of such a structure in situ, surrounded by other trabecular structures and enveloped by the cortical shell, could be different. However, our findings provide a stepping stone towards implementation of future whole bone studies of torsional failure and replace the erroneous use of torsion testing methods designed for axisymmetric and cylindrical specimens, conditions that nonhomogenous orthotropic materials such as bone do not satisfy.[23,24,41,42]

The contribution of trabecular morphometric indices averaged over the entire specimen and the region of failure to the overall torsional behavior of the specimen is limited compared to that obtained from the region with minimum BV/TV. This is partially explained by the lack of significant differences in the morphometric indices averaged over the entire specimen, the failure region, or the nonfailure region, suggesting that average indices provide a limited description of cancellous bone properties under torsion. In fact, the *minimum* properties overwhelmingly do so. This concept was investigated in compressive behavior of cancellous bone,[34] and it seems to hold true for torsional properties as well. Assessment of failure and nonfailure regions is only possible retrospectively, and as such is devoid of any predictive capability. However, these regions were investigated to verify whether any inherent differences in the trabecular microstructure existed between the areas that failed and those that did not.

We used whale vertebral cancellous bone because a large number of similar specimens can be obtained from a single vertebral body. While whale cancellous bone data cannot be a substitute for data on human bone, general trends probably hold true for human bone with similar microstructure (such as mostly platelike bone in distal femur) and density. Strength is a function of density, but the applicability of this technique to lower density bones must be studied. However, angular displacement is independent of density, so observations regarding displacement should hold true in trabecular bone with lower density. Human vertebral trabecular bone is much more porous than whale bone and is mostly comprised of rodlike elements. Further investigation of the torsional strength of mostly rodlike cancellous bones using this technique will be an important step, as the data presented here should not be extrapolated to lower density and more porous bones without validation. In a predominantly rodlike structure, alternative failure modes may be more prominent than those found in this study. The contribution of this work towards an understanding of bone quality in human bone is in the ability to measure applied loading correctly on cancellous bone and in elucidating the contribution of trabecular bone microstructure to its mechanical properties.

ACKNOWLEDGMENTS

The authors acknowledge Dr. Martin Stauber (Institute for Biomedical Engineering, University and ETH Zürich, Zürich) and Mr. Nipun D. Patel (Orthopedic Biomechanics Laboratory, Beth Israel Deaconess Medical Center, Harvard Medical School, Boston) for help with μCT image analysis.

REFERENCES

1. Chung H, Wehrli FW, Williams JL, et al. 1993. Relationship between NMR transverse relaxation, trabecular bone architecture, and strength. Proc Natl Acad Sci USA 90:10250–10254.
2. Ding M, Odgaard A, Linde F, et al. 2002. Age-related variations in the microstructure of human tibial cancellous bone. J Orthop Res 20:615–621.
3. Ikeda S, Tsurukami H, Ito M, et al. 2001. Effect of trabecular bone contour on ultimate strength of lumbar vertebra after bilateral ovariectomy in rats. Bone 28:625–633.
4. Kleerekoper M, Villanueva AR, Stanciu J, et al. 1985. The role of three-dimensional trabecular microstructure in the pathogenesis of vertebral compression fractures. Calcif Tissue Int 37:594–597.
5. Niebur GL, Feldstein MJ, Yuen JC, et al. 2000. High-resolution finite element models with tissue strength asymmetry accurately predict failure of trabecular bone. J Biomech 33:1575–1583.
6. Parfitt AM, Rao DS, Stanciu J, et al. 1985. Irreversible bone loss in osteomalacia. Comparison of radial photon absorptiometry with iliac bone histomorphometry during treatment. J Clin Invest 76:2403–2412.
7. Poodenphant J, Nielsen VA, Riis BJ, et al. 1987. Bone mass, bone structure and vertebral fractures in osteoporotic patients. Bone 8:127–130.
8. Rao DS, Parfitt AM, Kleerekoper M, et al. 1985. Dissociation between the effects of endogenous parathyroid hormone on adenosine 3′,5′-monophosphate generation and phosphate reabsorption in hypocalcemia due to vitamin D depletion: an acquired disorder resembling pseudohypoparathyroidism type II. J Clin Endocrinol Metab 61:285–290.
9. Recker RR. 1993. Architecture and vertebral fracture. Calcif Tissue Int 53 (Suppl 1) S139–S142.
10. Thomsen JS, Ebbesen EN, Mosekilde L. 1998. Relationships between static histomorphometry and bone strength measurements in human iliac crest bone biopsies. Bone 22:153–163.

11. Turner CH, Hsieh YF, Müller R, et al. 2001. Variation in bone biomechanical properties, microstructure, and density in BXH recombinant inbred mice. J Bone Miner Res 16:206–213.
12. Ulrich D, Hildebrand T, Van Rietbergen B, et al. 1997. The quality of trabecular bone evaluated with micro-computed tomography, FEA and mechanical testing. Stud Health Technol Inform 40:97–112.
13. Wachter NJ, Augat P, Hoellen IP, et al. 2001. Predictive value of Singh index and bone mineral density measured by quantitative computed tomography in determining the local cancellous bone quality of the proximal femur. Clin Biomech (Bristol, Avon) 16:257–262.
14. Nazarian A, Müller R. 2004. Time-lapsed microstructural imaging of bone failure behavior. J Biomech 37:55–65.
15. Nazarian A, Stauber M, Müller R. 2005. Design and implementation of a novel mechanical testing system for cellular solids. J Biomed Mater Res B Appl Biomater 73:400–411.
16. Müller R, Gerber SC, Hayes WC. 1998. Micro-compression: A novel technique for the nondestructive assessment of local bone failure. Technol Health Care 6:433–444.
17. Silva MJ, Gibson LJ. 1997. Modeling the mechanical behavior of vertebral trabecular bone: effects of age-related changes in microstructure. Bone 21:191–199.
18. Fyhrie DP, Schaffler MB. 1994. Failure mechanisms in human vertebral cancellous bone. Bone 15:105–109.
19. Halawa M, Lee AJ, Ling RS, et al. 1978. The shear strength of trabecular bone from the femur, and some factors affecting the shear strength of the cement-bone interface. Arch Orthop Trauma Surg 92:19–30.
20. Mitton D, Rumelhart C, Hans D, et al. 1997. The effects of density and test conditions on measured compression and shear strength of cancellous bone from the lumbar vertebrae of ewes. Med Eng Phys 19:464–474.
21. Sammarco GJ, Burstein AH, Davis WL, et al. 1971. The biomechanics of torsional fractures: the effect of loading on ultimate properties. J Biomech 4:113–117.
22. Stone JL, Beaupre GS, Hayes WC. 1983. Multiaxial strength characteristics of trabecular bone. J Biomech 16:743–752.
23. Bruyere Garnier K, Dumas R, Rumelhart C, et al. 1999. Mechanical characterization in shear of human femoral cancellous bone: torsion and shear tests. Med Eng Phys 21: 641–649.
24. Ford CM, Keaveny TM. 1996. The dependence of shear failure properties of trabecular bone on apparent density and trabecular orientation. J Biomech 29:1309–1317.
25. Hermann LR. 1965. Elastic Torsional Analysis of Irregular Shapes. Proc Am Soc Civil Eng 91:11–19.
26. Jepsen KJ, Akkus OJ, Majeska RJ, et al. 2003. Hierarchical relationship between bone traits and mechanical properties in inbred mice. Mamm Genome 14:97–104.
27. Kasra M, Grynpas MD. 2007. On shear properties of trabecular bone under torsional loading: Effects of bone marrow and strain rate. J Biomech 40:2898–2903.
28. Nazarian A, Bauernschmitt M, Eberle C, et al. 2007. Design and Validation of a Testing System to Assess Torsional Cancellous Bone Failure in Conjunction with Time-Lapsed Micro-Computed Tomographic Imaging. J Biomech 41:3496–3501.
29. Lorensen WE, Cline HE. 1987. Marching Cubes: A High Resolution 3D Surface Construction Algorithm. Comput Graph 21:163–169.
30. Levenston ME, Beaupre GS, van der Meulen MC. 1994. Improved method for analysis of whole bone torsion tests. J Bone Miner Res 9:1459–1465.
31. Dunn OJ, Clark V. 1969. Correlation Coefficients Measured on the Same Individuals. J Am Stat Assoc 64:366–377.
32. Meng XW, Rosenthal R, Rubin DB. 1992. Comparing correlated correlation coefficients. Quantitative Methods in Psychology 111:172.
33. Fenech CM, Keaveny TM. 1999. A cellular solid criterion for predicting the axial-shear failure properties of bovine trabecular bone. J Biomech Eng 121:414–422.
34. Nazarian A, Stauber M, Zurakowski D, et al. 2006. The interaction of microstructure and volume fraction in predicting failure in cancellous bone. Bone 39:1196–1202.
35. Ashman RB, Corin JD, Turner CH. 1987. Elastic properties of cancellous bone: measurement by an ultrasonic technique. J Biomech 20:979–986.
36. Ford C. 1996. Failure of the Human Proximal Femur: Material and Structural Perspectives. Ph.D., Massachusetts Institute of Technology, Cambridge, MA.
37. Stone J, Beaupre G, Hayes W. 1983. Multiaxial strength characteristics of trabecular bone. J Biomech 16:743–752.
38. Eswaran SK, Allen MR, Burr DB, et al. 2007. A computational assessment of the independent contribution of changes in canine trabecular bone volume fraction and microarchitecture to increased bone strength with suppression of bone turnover. J Biomech 40:3424–3431.
39. Mitton D, Rumelhart C, Hans D, et al. 1997. The effects of density and test conditions on measured compression and shear strength of cancellous bone from the lumbar vertebrae of ewes. Med Eng Phys 19:464–474.
40. Saha S, Gorman PH. 1981. Strength of human cancellous bone in shear and its relationship to bone mineral content. Trans Ortho Res Soc 27.
41. Brodt MD, Ellis CB, Silva MJ. 1999. Growing C57Bl/6 mice increase whole bone mechanical properties by increasing geometric and material properties. J Bone Miner Res 14:2159–2166.
42. Tommasini SM, Morgan TG, van der Meulen M, et al. 2005. Genetic variation in structure-function relationships for the inbred mouse lumbar vertebral body. J Bone Miner Res 20: 817–827.